

Device Modeling and Simulation of the Performance of $\text{Cu}(\text{In}_{1-x}\text{Ga}_x)\text{Se}_2$ Solar Cells

Jiyon Song^a, Sheng S. Li^a, C.H. Huang^b, O.D. Crisalle^c, and T.J. Anderson^c

a. Department of Electrical and Computer Engineering,

c. Department of Chemical Engineering,

University of Florida, Gainesville, FL 32611, U.S.A.

b. Department of Electrical Engineering

National Dong Hwa University, Taiwan

Abstract

Device modeling and simulation studies of a $\text{Cu}(\text{In}_{1-x}\text{Ga}_x)\text{Se}_2$ (CIGS) thin film solar cell have been carried out. A variety of graded band-gap structures, including space charge region (SCR) grading, back surface region grading, and double grading of the CIGS absorber layer, are examined. The device physics and performance parameters for different band-gap profiles were analyzed. Based on the simulation results, an optimal graded band-gap structure for the CIGS solar cell is proposed. The performance of the optimally graded band-gap cell is superior to that of the uniform band-gap cell. The SCR grading of the CIGS absorber layer improves the open-circuit voltage (V_{oc}) without significantly sacrificing the short-circuit current (J_{sc}) compared to the uniform band-gap CIGS. The back surface grading enhances both V_{oc} and J_{sc} . An optimal graded band-gap profile, such as a double grading consisting of the SCR grading and back surface grading, improves significantly the efficiency up to 19.83% AM1.5G compared to the uniform band-gap profile with 15.42% efficiency. A comparison of the simulation results with published data for the CIGS cells shows an excellent agreement of photo-current density- voltage and quantum efficiency characteristics.

Keywords: Device modeling, thin Film solar cell; $\text{Cu}(\text{In,Ga})\text{Se}_2$ (CIGS), graded band-gap, open-circuit voltage (V_{oc}), short-circuit current (I_{sc}), conversion efficiency.

* Corresponding author: *E-mail address:* shengli@eng.ufl.edu (Sheng S. Li).

1. Introduction

Much information is available in the literature regarding single-junction $\text{Cu}(\text{In}_{1-x}\text{Ga}_x)\text{Se}_2$ (CIGS) solar cells. Increasing the open-circuit voltage (V_{oc}) to improve the overall performance of CIGS cells is highly desirable because it minimizes the interconnection losses in the manufacture of cell modules. When alloying the CuInSe_2 (CIS) with Ga to form CIGS thin films, the wider band-gap energy of the CIGS absorber layer can potentially better match the solar spectrum, as well as increase the V_{oc} of the fabricated cells, at the expense of a reduction in the value of the short-circuit current density (J_{sc}). Introducing a spatial variation of the Ga content within the CIGS layer, the band-gap profile can be optimized to increase the photon absorption and carrier diffusion. Furthermore, the Ga profile can be adjusted to optimize the CIGS absorber band gap profile, and hence improve the V_{oc} and J_{sc} values. Thus, band-gap engineering geared to controlling the spatial distribution of the Ga content in the absorber layer can lead to enhancing the overall performance of CIGS cells.

In this paper, device modeling and numerical simulations of CIGS cells are conducted to analyze the impacts of various band-gap profiles for the CIGS layers on the performance parameters of the cells. Such modeling works will provide insight into which structures may be desired. The investigation focuses on the study of the effect on performance caused by various band-gap profiles in the space charge region (SCR) and in the back surface region of the absorber layer. Seven band gap profiles are analyzed, including the baseline case of a uniform band-gap profile. Based on the simulation

results, an optimal graded band-gap structure for the CIGS cell is proposed. The simulation results of the optimized cell are compared to the reported experimental data. Additionally, the performance parameters of simulated results for CIGS cells with comparable grading structures in the absorber layers were found in excellent agreement with the published data.

2. Cell Structure and Material Parameters

The schematic energy-band diagram under equilibrium condition for a typical ZnO/CdS/CIGS solar cell with a uniform band-gap profile is illustrated in Figure 1. An inverted surface layer, which is referred to as an ordered vacancy compound (OVC), is present between the CdS and CIGS layers in the diagram. Schmid *et al.* [1] have demonstrated the existence of such a thin OVC, In-rich *n*-type layer, on the surface of the as-deposited CIGS films, and assigned to it the stoichiometry of $\text{CuIn}_2\text{Se}_{3.5}$ or CuIn_3Se_5 . However, some literatures [2-3] revealed that the compound of In-rich surface layer might not be the OVC and used a more general term ‘surface defect layer’ for this thin *n*-type layer. The inverted surface layer is considered to be beneficial to the performance of CIGS cells because the electrical junction is shifted away from the high-recombination interface between the CdS and CIGS layer, and hence the recombination rate is reduced. However, the properties of the surface defect layer such as high defect densities and high resistivity might lead to deteriorating the cell performance.

The CIGS cell structure considered in this study consists of the following material layers: *n*-ZnO, *n*-CdS, high-recombination interface, inverted surface, *p*-CIGS absorber, and a Mo on glass substrate. The computer simulation tool *AMPS-1D* (Analysis of

Microelectronic and Photonic Structures) [4] was employed by specifying as input values the semiconductor parameters in each layer of the cell structure. The division of the layers for the cell structure is limited to the simplified device structure described above because of the limited knowledge available on the semiconductor parameters in each layer and uncertainties in the interface and junction properties arising from possible interdiffusion and reaction during the cell processing. The band gap of the CIGS absorber is engineered through the addition of a Ga profile. The anticipated changes in the physical properties of the CIS films with the addition of Ga include an increase in band gap, which mainly shifts the position of the conduction-band minimum [5], as well as changes in the hole concentration [6], bulk defect densities [7], absorption coefficients, and electron affinities. The room temperature mobility was found to remain nearly constant while varying the Ga content over a wide range [6].

Except when otherwise mentioned, in the simulation studies an inverted surface layer with a thickness $t = 30$ nm, electron mobility $\mu_n = 10$ cm²/V-s, net carrier density $n = 10^{12}$ cm⁻³, and band gap $E_g = 1.3$ eV is inserted between the CdS and CIGS layers. Also, an interface layer with a high density of effective recombination centers is placed at the metallurgical junction between the inverted surface layer and the CdS layer. The total thickness of the absorber layer is maintained at 2 μ m for all cases, including the various graded band-gap structures studied. In order to model an effective recombination center, a deep level defect is placed in the middle of the band gap of (i) the CdS layer, (ii) the high-recombination interface layer, (iii) the inverted surface layer, and (iv) the SCR of the CIGS absorber. To examine the effects of band-gap gradient on the device performance, most of the material parameters used in the simulations are maintained

unchanged, except that the band gaps, electron affinities, and optical absorption coefficients are varied with the Ga mole fraction in the CIGS films.

3. Effect of Graded Band-gaps on Cell Performance

First, a simulation study of uniform band-gap CIS and CIGS cells is carried out to establish a baseline for comparison. Two representative band-gaps, namely 1.04 eV for CIS and 1.20 eV for CIGS, are considered. The simulation results are shown in Table 1. It is noted that the $\text{Cu}(\text{In}_{1-x}\text{Ga}_x)\text{Se}_2$ cell with composition $x \approx 0.32$ and $E_g \approx 1.20$ eV [8] has a higher V_{oc} and a smaller J_{sc} than the CuInSe_2 cell corresponding to $x \approx 0$ and $E_g \approx 1.04$ eV, due to the smaller absorption coefficients and the reduction in the absorption of longer-wavelength photons. The effect of higher Ga-content of uniform band-gaps is not further analyzed because it has been reported in the literature that the device performance degraded when the Ga content in the $\text{Cu}(\text{In}_{1-x}\text{Ga}_x)\text{Se}_2$ films exceeds 30 - 40%, *i.e.*, when $x > 0.3 - 0.4$ [9].

Second, a simulation study of the dependence of the cell performance on the band gap in the SCR of CIGS absorbers is carried out. The recombination rate in the SCR, which controls the V_{oc} of the CIGS cell, can be reduced by increasing the barrier height via the increase of the SCR band-gap. This improves the V_{oc} , but a small loss of J_{sc} might be expected if the wider band-gap region is not sufficiently thin. The dependence of V_{oc} on the band gap in the SCR of CIGS cells has been reported [10]. In the simulation model, the SCR is composed of a series of layers of different band-gaps. The bottom-most layer in the SCR matches the band gap of 1.04 eV of the underlying CIGS bulk material, and the subsequent SCR layers located above linearly increase until

reaching a wide band-gap end-point value (EPV) varying from 1.16 to 1.35 eV. More specifically, the EPV indicates the band gap of the SCR layer next to the inverted surface layer. The band-gaps of the inverted surface layer and of the remaining region of the CIGS bulk layer are maintained at $E_g = 1.30$ eV and 1.04 eV, respectively. The simulation results are shown in Figure 2, where the resulting performance parameters of V_{oc} , J_{sc} , fill factor (F.F.), and efficiency (η) are shown as a function of the EPV of the band gap in the SCR. The value of V_{oc} in Figure 2 (a) increases with increasing end-point band-gap in the SCR, improving from ~ 537 to ~ 551 mV, while the value of J_{sc} in Figure 2 (b) decreases slightly from ~ 37.9 to ~ 37.6 mA/cm². When comparing the performance of the graded band-gap cells reported in Figure 2 with the performance of the uniform band-gap CIS cell reported in Table 1, it is apparent that SCR grading improves the V_{oc} without significantly decreasing the J_{sc} . The F.F. values of the graded cells shown in Figure 2 (c) are also higher than that of the uniform band-gap CIS cell. The figure shows that different EPV values produce different F.F. values, but that the relationship is not monotonic. This is a consequence of the conduction-band offset between the inverted surface and CIGS layers. The value of η in Figure 2 (d) increases from $\sim 15.3\%$ to a maximum value of $\sim 16.0\%$ at an EPV value of ~ 1.30 eV. Comparing the efficiencies in Figure 2 (d) with the efficiency of the uniform-gap CIS cell in Table 1, it can be concluded that band gap grading in SCR has a favorable effect on the final conversion efficiency.

Third, a simulation study was conducted to evaluate the effect of graded band-gap profiles of the CIGS absorber on the performance of the cells. A total of seven band gap profile cases are considered, as shown in Table 2. The simulation results for each case

yield the performance parameters η , V_{oc} , J_{sc} , and F.F reported in columns 3 to 6 of the table. The band-gap profile of Case 1 is the baseline, featuring a uniform band-gap of 1.16 eV for the entire CIGS absorber layer. In Case 2, a back surface field (BSF) is formed by the normal grading, where the band gap is linearly increased towards the back, and in Case 3, a step grading is used, where a wider band-gap layer is placed in the back. In Case 4, a wider band-gap CIGS layer of 1.30 eV, decreasing linearly to 1.16 eV, is placed entirely in the SCR. In Case 5 and 6, a double graded band-gap structure using the wider band-gap layer in the SCR and in the back surface region of the absorber is introduced. Comparing the performance of the cell in Case 1, both the V_{oc} and J_{sc} with either a normal (Case 2) or step (Case 3) back surface grading are improved simultaneously, and hence the conversion efficiency is also increased, as shown in Table 2. The double graded band-gap structure of Case 6 realizes a high conversion efficiency of 18.39% AM1.5G. Figure 3 illustrates the schematic energy band diagram under equilibrium condition for Case 6 with a double band-gap grading. In this figure, a quasi-electrical field [11] can be established by the band-gap gradient with the incorporation of a high Ga content in the back region (near the Mo contact) of the CIGS absorber layers by reducing the back surface recombination and increasing the effective minority-carrier diffusion length. This results in an efficient carrier collection in the CIGS cells, and thus both the V_{oc} and J_{sc} are enhanced. The same trend was observed when comparing the performance of the cells in Cases 5 and 6 with that in Case 4. Case 7 is analogous to Case 6, except that the doping density in the CdS layer is increased to $6 \times 10^{17} \text{ cm}^{-3}$ and the deep-level defect densities are assumed to be equal to zero in the CIGS absorber. The result yields a maximum conversion efficiency of 19.83% for this cell.

In summary, a proper band-gap grading consisting of a wider band-gap CIGS layer in the SCR and a back surface grading are capable of significantly improving the performance of the CIGS cells. In the simulation studies the band gaps in the SCR and in the back region and the thickness of the back surface grading layers are varied to achieve the optimal performance through reducing the carrier recombination and increasing the carrier collection for the given material parameters and device structure. Comparing the performance of a uniform band-gap cell (Case 1) with the graded band-gap cells (Case 5 and Case 6), the benefit of band-gap grading for the CIGS solar cells is clearly demonstrated.

4. Comparison with Experimental Data

Attempts are made to compare the simulation results with reported experimental data for the CIGS cells. The measured values are taken from the photo- current density-voltage (J-V) and normalized quantum efficiency (Q.E.) curves of an experimental CIGS cell with 18.8% efficiency under standard conditions produced at the National Renewable Energy Laboratory (NREL) [12-13]. The performance of this experimental cell is compared with the simulated results of Cases 6 and 7 in Table 2, and the results are shown in Figures 4 and 5, where the solid line represents the simulated cell of Case 6, the dashed line represents the simulated cell of Case 7, and the solid circles denote the experimental values. Figure 4 shows that the photo- J-V curve for Case 6 closely matches the experimental curve for the NREL CIGS cell. The photo- J-V values obtained from the simulation of Case 7 suggest that a higher efficiency is possible. Figure 5 shows a comparison of the simulated Q.E. curve for Case 6 with the

experimental curve. Good agreement was also observed in this case in the wavelength (λ) range of $0.5 \mu\text{m} \leq \lambda \leq 1.2 \mu\text{m}$.

A separate analysis is carried out to fit the performance of the simulated parameters with data available in the published literature for CIGS cells. Dullweber *et al.* have reported experimental results for band-gap grading in CIGS cells [10,14]. The band-gap structure of the CIGS absorber layer in Table 3 is based on the Auger depth profile reported by Dullweber *et al.* [10], which allows defining the layer dimensions and compositions for the simulation model. For the simulation study, the depth profile is represented by an equivalent band-gap profile in the CIGS absorber using the equation $E_g(y) [\text{eV}] = 1.02 + 0.67 y + 0.11 y (y-1)$ proposed in [15], where the variable y denotes the ratio of Ga/(Ga+In). The resulting band-gap profile reveals a double-graded CIGS absorber layer with linearly graded band-gap structures in the SCR and in the CIGS bulk layers, as shown in Table 3, and is used as a set of input parameters for the simulation study. This notch structure is a particular case of double grading. Theoretical analysis and simulation studies of this structure have been reported [16]. The measured data are also taken from the J-V curve given in [10]. The key parameters used in fitting the simulation results to the experimental values are the defect density in the inverted surface layer, the defect densities of the mid-gap deep-level in the SCR, and the defect and hole densities in the CIGS absorber. The results are shown in Figure 6, where the simulated values are plotted using a solid line, and the experimental values are indicated by the solid circles. Although the simulated F.F. is slightly higher than the experiment, excellent agreement was observed in the J-V curve.

Finally, another work by Dullweber *et al.* [14] for CIGS cells with a normal or reverse graded absorber is considered for fitting the simulation results to experimental values. An absorber with normal grading profile is one where the band gap is increased linearly from the front to the backside in the entire absorber, while the absorber with reverse grading profile is one where the band gap is decreased linearly from the front to the back. To investigate these linearly graded structures via simulation, the composition depth profiles of the CIGS absorber given in [14] were used for the calculation of the band-gap profiles for the CIGS absorber. From the represented band-gap profiles, an absorber structure with normal grading is increased linearly from the front band-gap of 1.03 eV to the backside band-gap of 1.22 eV, while an absorber profile with reverse grading is decreased from 1.24 eV to 1.06 eV. Also, a uniform band-gap profile of 1.14 eV is considered. Experimental performance parameters are also extracted from [14] for the cases of normal, reverse, and uniform grading, and are compared with the simulated results. The major parameters used in fitting the simulated results to the experimental values are as described in the preceding paragraph. The results are shown in Figure 7, where the solid circle and triangle denote the simulated values and experimental data, respectively. The x-axis indicates CIGS absorber band-gap profiles consisting of the reverse grading, uniform, and normal grading from left to right. It is noted that from Figure 7 (a) V_{oc} is found to decrease from 565 to 509 mV (a change of 56 mV), from the reverse to the normal grading, while the value of J_{sc} increases from 32.5 to 37.5 mA/cm² (a change of 5 mA/cm²) as shown in Figure 7 (b). These trends are also found in the experimental values. Excellent agreement was obtained on the performance parameters

V_{oc} , J_{sc} , and F.F. Even though the values of η in the simulation are slightly higher than their experimental counterparts, a reasonable fit is nevertheless obtained.

5. Summary and Conclusions

Comprehensive device modeling and numerical simulation studies for single-junction CIGS thin film solar cells have been carried out using the AMPS-1D device simulation program, including various absorber band-gap profiles. A detailed analysis of the graded band-gap structures for the CIGS cells has been presented. It is shown that band-gap grading using a wide band-gap layer in the SCR and/or back surface grading using the gradient of Ga content in the CIGS absorber layer greatly improve the performance of single-junction CIGS cells. Additionally, studies to fit the simulation results with the reported experimental data show reasonable agreement in the J-V and Q.E. curves between the modeling and the experimental data.

Acknowledgements

This work was supported by the DOE/NREL High Performance PV Program under Contract No. AAT-1-30620-11. The authors acknowledge the use of AMPS-1D program developed by Dr. Fonash's group of Pennsylvania State University in all the simulations reported in this paper.

References

- [1] Schmid D., Ruckh M., Grunwald, F., Schock H.W. Chalcopyrite/defect chalcopyrite heterojunctions on the basis of CuInSe₂. J. Appl. Phys. 1993;73:2902-2909.
- [2] Herberholz R., Rau U., Schock H.W., Haalboom T., Gödecke T., *et al.* Phase segregation, Cu migration and junction formation in Cu(In,Ga)Se₂. European Physical J. Appl. Phys. 1999;6:131-139.
- [3] Guillemoles J., Haalboom T., Gödecke T., Ernst F., Cahen D. Phase and interface stability issues in chalcopyrite-based thin film solar cells. Mat. Res. Soc. Symp. Proc. 1998;485:127-132.
- [4] Zhu H., Kalkan A.K., Hou J., Fonash S.J. Application of AMPS-1D for solar cell simulation. AIP Conf. Proceedings 1999;462:309-314.
- [5] Wei S.H., Zunger A. Band offsets and optical bowings of chalcopyrites and Zn-based II-VI alloys. J. Appl. Phys. 1995;78:3846-3856.
- [6] Schroeder D.J., Hernandez J.L., Rockett A.A. Point defects and hole transport in epitaxial CuIn_{1-x}Ga_xSe₂. 11th Int. Conf. on Ternary and Multinary Compounds 1999:749-752.
- [7] Hanna G., Jasenek A., Rau U., Schock H.W. Influence of the Ga-content on the bulk defect densities of Cu(In,Ga)Se₂. Thin Solid Films 2001;387:71-73.

- [8] Wei S.H., Zhang S.B., Zunger A. Effects of Ga addition to CuInSe₂ on its electronic, structural, and defect properties. Appl. Phys. Letters 1998;72:3199-3201.
- [9] Walter T., Menner R., Ruckh M., Kaser L., Schock H.W. Parameter studies and analysis of high efficiency Cu(In,Ga)Se₂ based solar cells. Proc. 22nd IEEE PVSC Conf. 1991:924-929.
- [10] Dullweber T., Hanna G., Rau U., Schock H.W. A new approach to high-efficiency solar cells by band gap grading in Cu(In,Ga)Se₂ chalcopyrite semiconductors. Solar Energy Materials & Solar Cells 2001;67:145-150.
- [11] Koremer H., RCA Review 1957;18:332.
- [12] Contreras M.A., Egaas B., Ramanathan K., Hiltner J., Swartzlander A., Hasoon F., Noufi R., Progress toward 20% efficiency in Cu(In,Ga)Se₂ polycrystalline thin-film solar cells. Progress in Photovoltaics: Research & Application 1999;7:311-316.
- [13] <http://www.nrel.gov/measurements/voltage.html>:
- [14] Dullweber T., Hanna G., Shams-Kolahi W., Schwartzlander A., Contreras M.A., Noufi R., Schock H.W. Study of the effect of gallium grading in Cu(In,Ga)Se₂. Thin Solid Films 2000;361-362:478-481.
- [15] Dullweber T., Rau U., Contreras M.A., Noufi R., Schock H.W. Photogeneration and carrier recombination in graded gap Cu(In,Ga)Se₂ solar cells. IEEE Trans. Electron Devices 2000;47(12):2249-2254.

- [16] Dhingra A., Rothwarf A. Computer simulation and modeling of the graded bandgap CuInSe₂/CdS solar cell. Proc. 23rd IEEE PVSC Conf. 1993:475-480.

Figure Captions

- Figure 1. The schematic energy-band diagram of a typical ZnO/CdS/CIGS solar cell under equilibrium condition.
- Figure 2. The dependence of cell performance parameters on the band-gap energy in the space charge region (SCR) of CIGS cells.
- Figure 3. The schematic energy-band diagram of a CIGS cell with a double band-gap grading profile under equilibrium condition.
- Figure 4. The photo- current density- voltage (J-V) curves for the simulated results (solid and dashed lines) and the reported experimental data (solid circles) [12-13].
- Figure 5. The normalized quantum efficiency (Q.E.) for the simulated results (solid line) and the reported experimental values (solid circles) [12].
- Figure 6. The photo- current density-voltage (J-V) curves for the simulated results (solid line) and the published data (solid circles) [10].
- Figure 7. A comparison of the performance parameters for the simulated results (circles) and the published data (triangles) [14].

Table Captions

Table 1. Simulated performance parameters of the $\text{Cu}(\text{In}_{1-x}\text{Ga}_x)\text{Se}_2$ for $x = 0$ ($E_g = 1.04$ eV), and $\text{Cu}(\text{In}_{1-x}\text{Ga}_x)\text{Se}_2$ for $x = 0.32$ ($E_g \approx 1.20$ eV) solar cells with a uniform absorber band-gap profile.

Table 2. Simulated performance parameters of the CIGS solar cells with various absorber band-gap profiles.

Table 3. The energy band-gap profile of the CIGS absorber layer used in simulation.

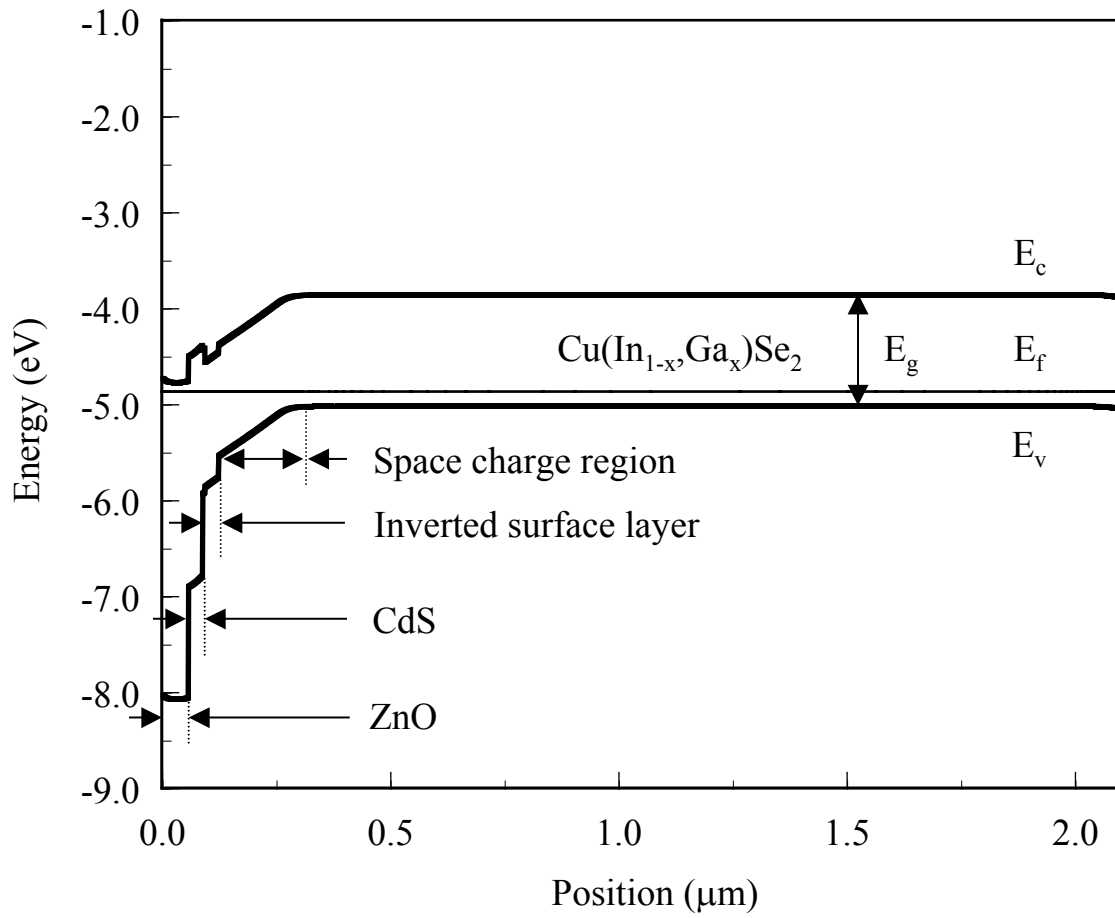


Figure 1. The schematic energy-band diagram of a typical ZnO/CdS/CIGS solar cell under equilibrium condition.

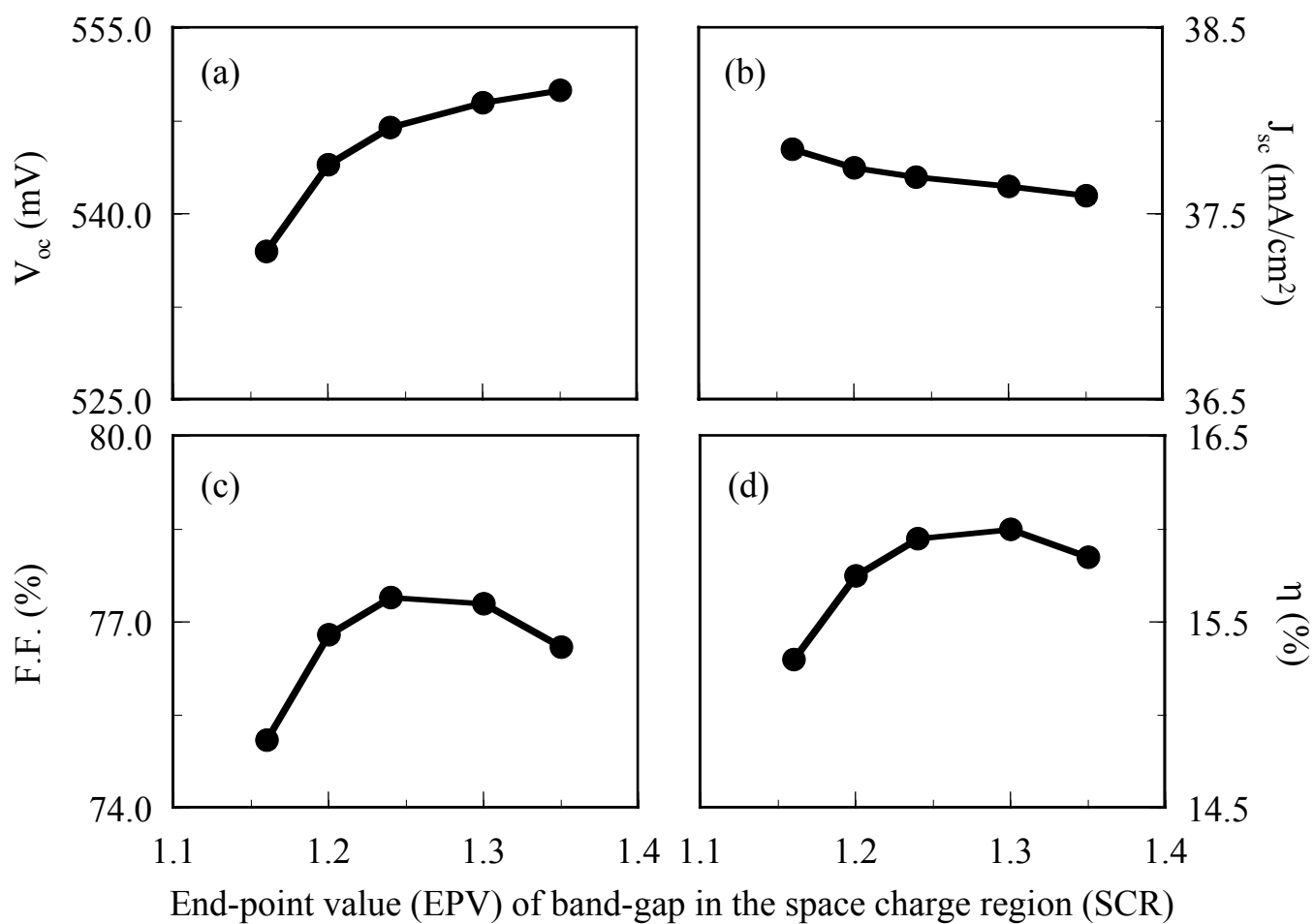


Figure 2. The dependence of cell performance parameters on the band-gap energy in the space charge region (SCR) of CIGS cells.

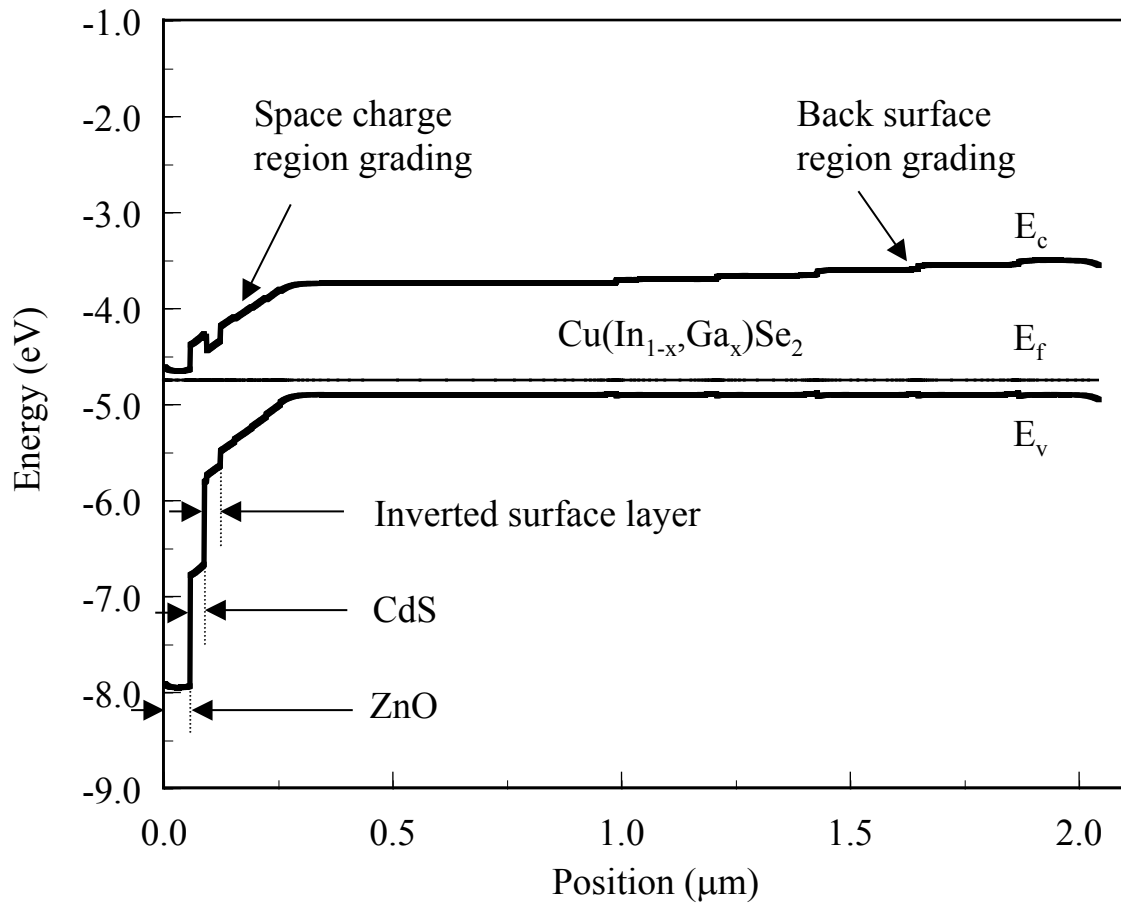


Figure 3. The schematic energy-band diagram of a CIGS cell with a double band-gap grading profile under equilibrium condition.

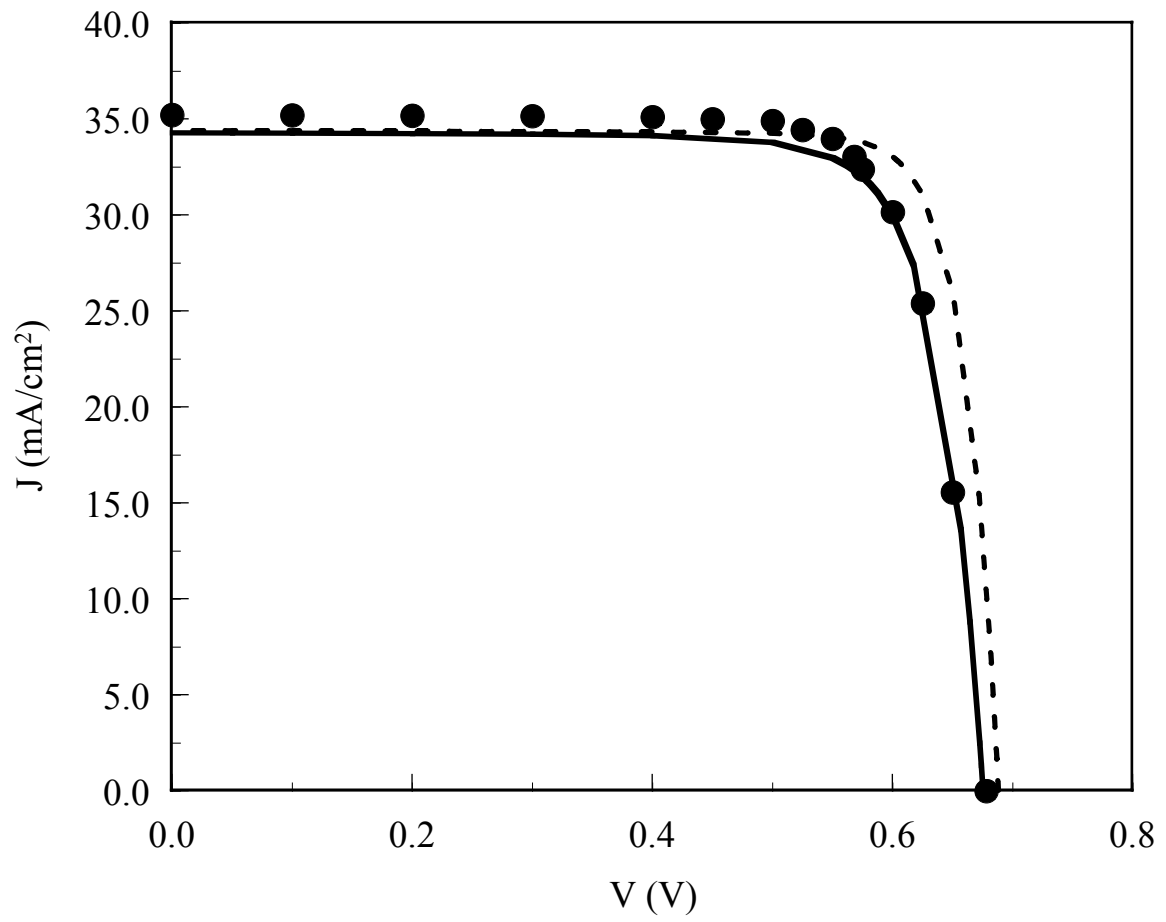


Figure 4. The photo- current density-voltage (J-V) curves for the simulated results (solid and dashed lines) and the reported experimental data (solid circles) [12-13].

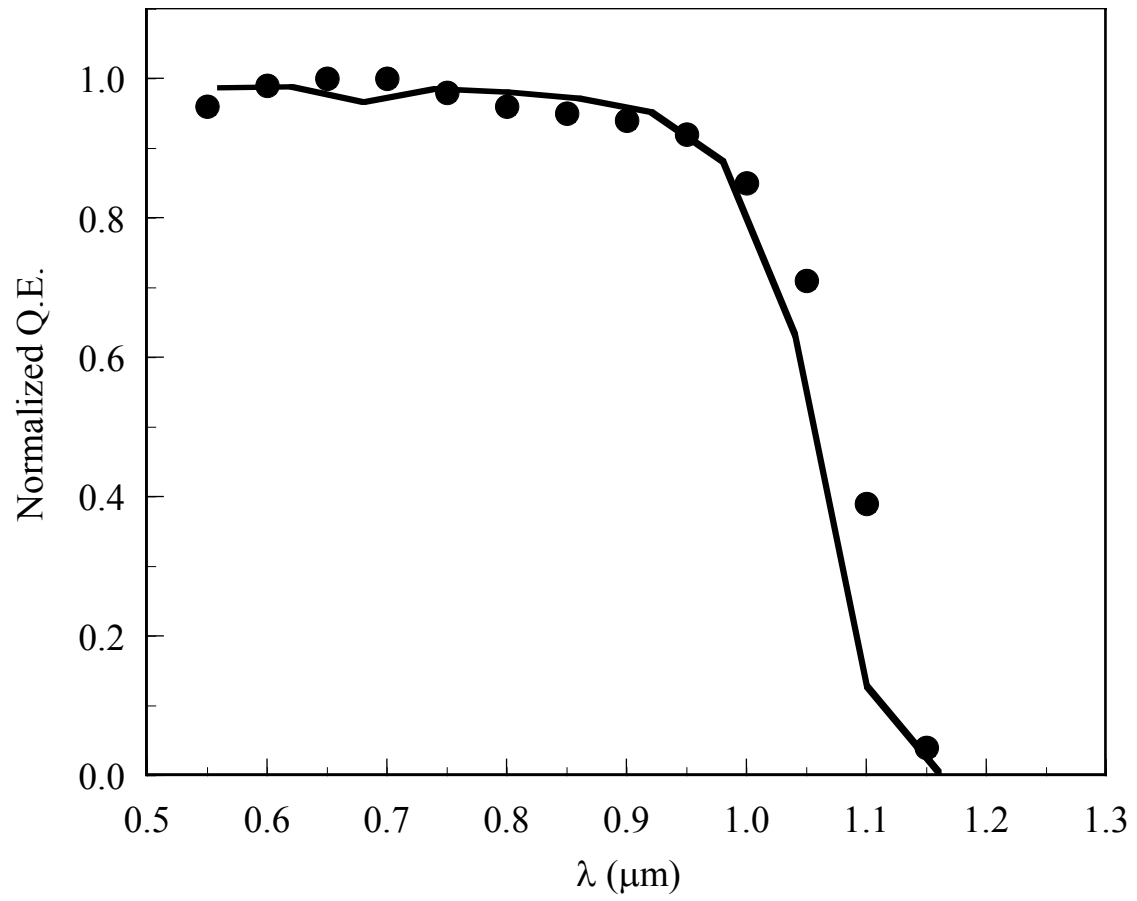


Figure 5. The normalized quantum efficiency (Q.E.) for the simulated results (solid line) and the reported experimental values (solid circles) [12].

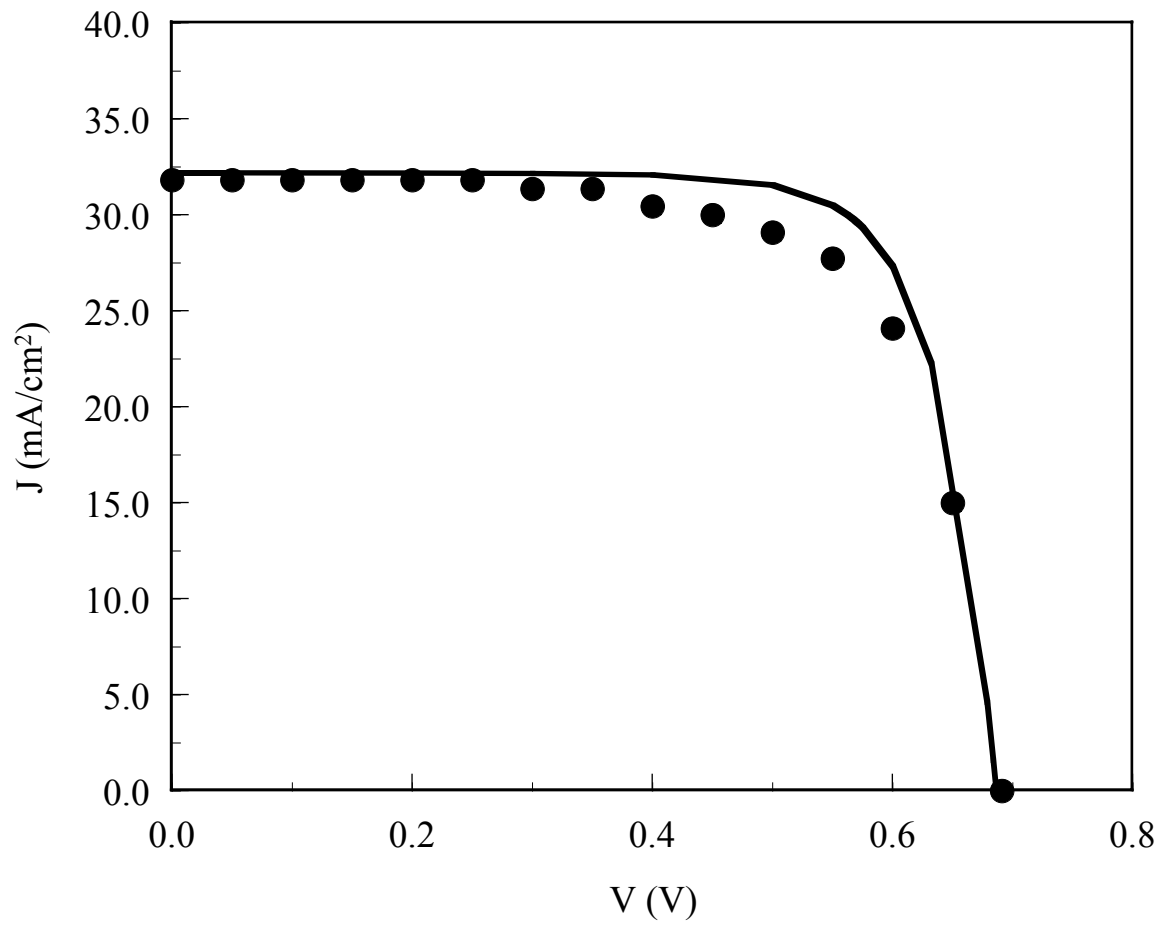


Figure 6. The photo- current density-voltage (J-V) curves for the simulated results (solid line) and the published data (solid circles) [10].

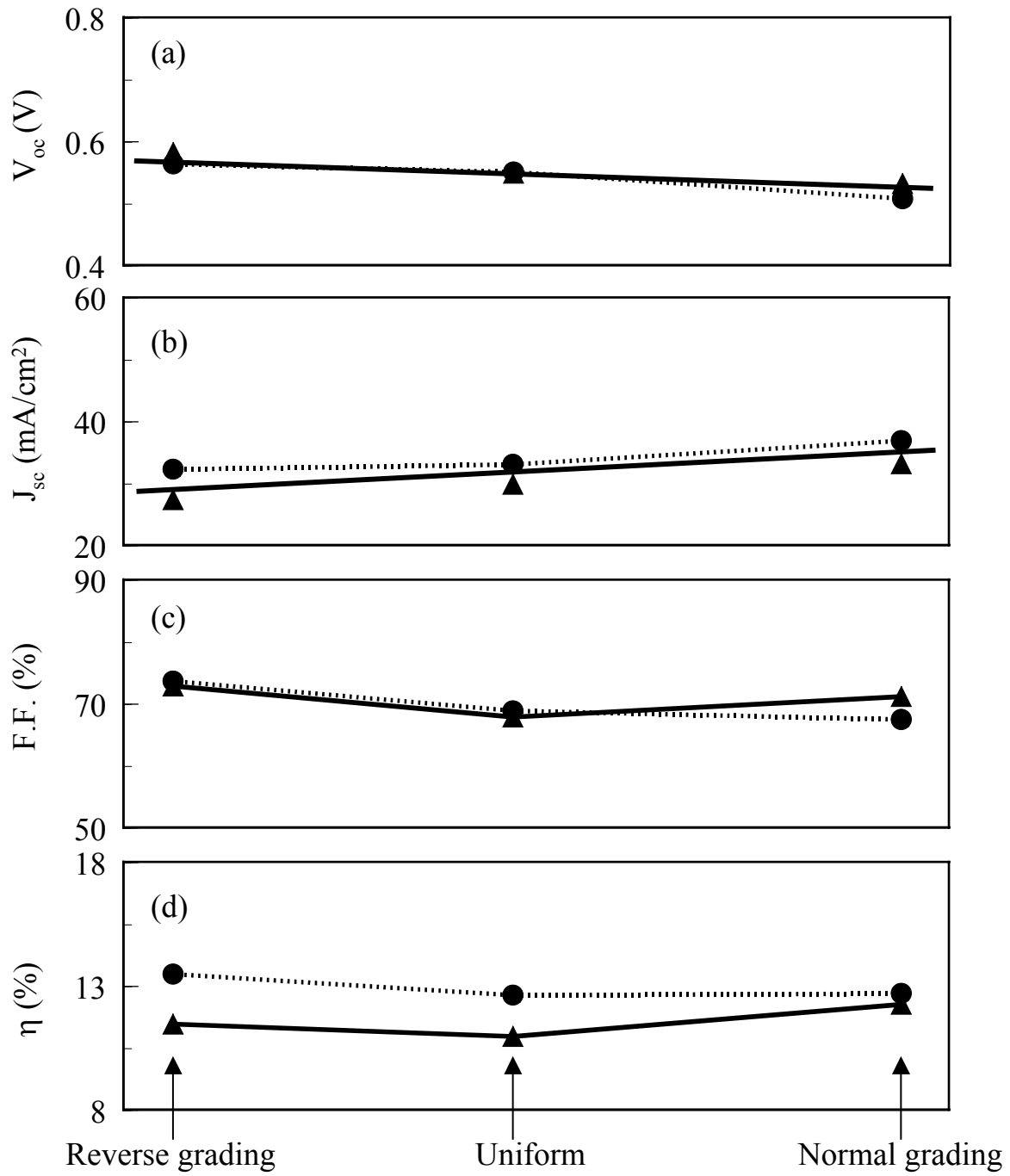


Figure 7. A comparison of the performance parameters for the simulated results (circles) and the published data (triangles) [14].

Table 1. Simulated performance parameters of the $\text{Cu}(\text{In}_{1-x}\text{Ga}_x)\text{Se}_2$ for $x = 0$ ($E_g = 1.04$ eV), and $\text{Cu}(\text{In}_{1-x}\text{Ga}_x)\text{Se}_2$ for $x = 0.32$ ($E_g \approx 1.20$ eV) solar cells with a uniform absorber band-gap profile.

	x	E_g (eV)	η (%)	V_{oc} (mV)	J_{sc} (mA/cm ²)	F.F. (%)
CuInSe_2	0	1.04	13.00	500	38.01	68.4
$\text{Cu}(\text{In}_{1-x}\text{Ga}_x)\text{Se}_2$	0.32	1.20	15.77	655	32.27	74.6

Table 2. Simulated performance parameters of the CIGS solar cells with various absorber band-gap profiles.

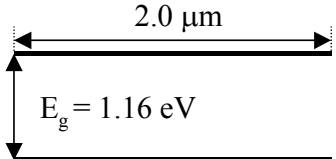
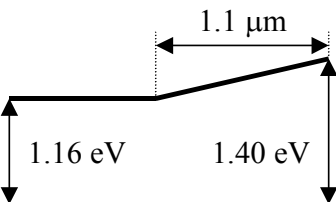
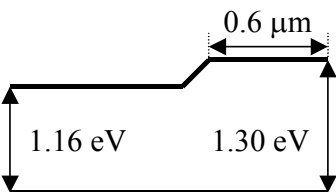
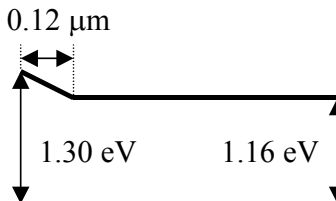
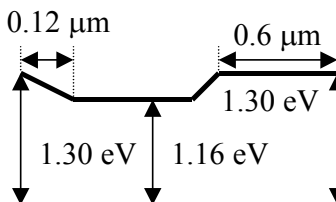
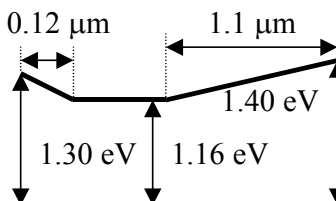
	Band-gap profile	η (%)	V_{oc} (mV)	J_{sc} (mA/cm ²)	F.F. (%)
Case 1		15.42	617	34.05	73.4
Case 2		15.72	622	34.61	73.1
Case 3		15.81	620	34.77	73.3
Case 4		17.57	658	33.55	79.6
Case 5		18.34	669	34.46	79.6
Case 6		18.39	675	34.31	79.4
Case 7	Same profile as Case 6	19.83	688	34.42	83.8

Table 3. The energy band-gap profile of the CIGS absorber layer used in simulation.

